

In-situ measurement of the scintillation light attenuation in liquid argon in the GERDA Experiment

N. Barros^{a,1}, A.R. Domula^a, B. Lehnert^{a,2}, B. Schneider^{a,*}, K. Zuber^{a,b}

^a*Institute of Nuclear and Particle Physics, TU Dresden, Dresden, Germany*

^b*MTA Atomki, Institute for Nuclear Research, Hungarian Academy of Sciences, Debrecen, Hungary*

Abstract

The GERDA experiment searches for the neutrinoless double beta ($0\nu\beta\beta$) decay in ^{76}Ge in order to probe whether the neutrino is a Majorana particle and to shed light on the neutrino mass ordering. For investigating such a rare decay it is necessary to minimize the background of the experiment. In Phase II of the GERDA experiment the scintillation light of liquid argon (LAr) is used as an additional background veto. In order to estimate the efficiency of such a LAr veto it has to be known how far the scintillation light can travel within the LAr. A dedicated setup was built to measure the attenuation length of the scintillation light in the LAr in-situ within the cryostat of GERDA. The setup is composed of a steel tube with a photomultiplier tube (PMT) at one side and a moveable ^{90}Sr source at the other side to measure the light intensity at different distances between source and PMT.

Furthermore, a sophisticated simulation was developed in order to determine the solid angle correction as well as the background for this measurement, both are needed for the analysis. Additionally, a set of simulation data was generated to confirm the analysis which is performed for the measured data afterwards and to find a combination of simulation parameters that matches the measured data. The analysis results in an absorption length of $15.79 \pm 0.70(\text{stat})_{-3.14}^{+1.42}(\text{syst})$ cm under the assumption of a scattering length of 70 cm at 128 nm. The simulation matching best was produced with an absorption length of 18 cm and a light yield of 2500 γ/MeV .

Keywords: liquid argon, scintillation, light yield, attenuation, absorption, scattering, Cherenkov light, steel reflectivity

1. Introduction

The Germanium detector array (GERDA) is an experiment located in the underground laboratory LNGS (Laboratori Nazionali del Gran Sasso) and searches for the $0\nu\beta\beta$ decay in ^{76}Ge [1]. GERDA operates isotopically enriched HPGe (high purity germanium) detectors in liquid argon (LAr), which serves as a cooling and shielding against external radiation.

The current limit of GERDA on the half live of the $0\nu\beta\beta$ decay of ^{76}Ge is $T_{1/2} > 0.9 \cdot 10^{26}$ yr (90% C.L.) [2]. The measurement of such a rare decay requires to minimize the background of the experiment. One of the major improvements in GERDA Phase II is a scintillation light detector veto surrounding the HPGe crystals. Hence, any energy deposition in LAr within this device can be used as a veto and thus helps to suppress background. This includes intrinsic impurities in LAr that could mimic the $\beta\beta$ decay as well as nuclides produced by cosmogenic activation

inside the detectors and other natural abundant nuclides inside the surrounding material like detector holders and cables. For this purpose, the argon volume surrounding the germanium detectors was instrumented with a system consisting of a combination of reflectors, wavelength shifters (WLS) and PMTs.

The scintillation light in LAr is created by the emission of a de-excitation photon from either a singlet or a triplet state. The creation ratio of singlet to triplet state is about 0.3 for electrons. While the transition of the singlet state is allowed (4 – 7 ns), the triplet state is forbidden (1.0 – 1.7 μs), resulting in different decay times [11].

In case the excited LAr molecule in the singlet or triplet state collides with impurities in the LAr, such as Oxygen or Nitrogen, it can de-excite non-radiatively, decreasing the light yield and thus mainly the lifetime of the triplet state. Furthermore, Oxygen can also absorb scintillation photons directly, which decreases the light yield as well as the absorption length even more.

Consequently the scintillation light cannot travel infinite inside the LAr but is attenuated during its propagation due to impurities in the LAr [3–5], providing a limit on the effective active volume of the LAr veto. In order to estimate the efficiency of the LAr veto the attenuation length of the scintillation light was measured inside the GERDA cryostat.

*Corresponding author

Email address: Birgit.Schneider@tu-dresden.de

(B. Schneider)

¹Present Address: Department of Physics & Astronomy, University of Pennsylvania, Philadelphia, USA

²Present Address: Lawrence Berkeley National Laboratory, Berkeley, USA

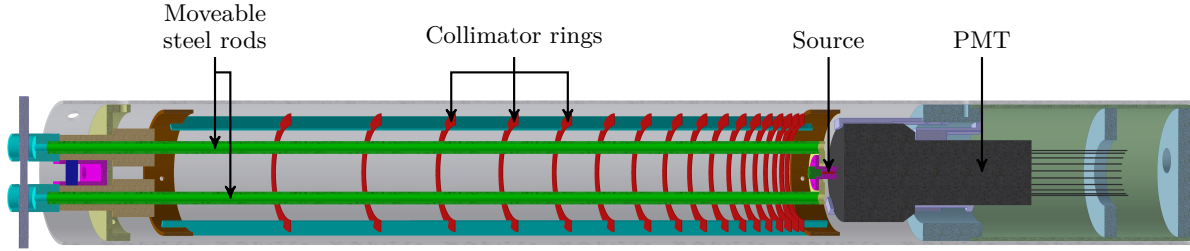


Figure 1: CAD drawing of the setup for the attenuation measurement. The setup is completely made of stainless steel with the exception of the PMT holder, which is composed of PTFE. The PMT is fixed in one side of the setup, while the source can be moved on the other side to adjust the distance between them. The source is located in a source holder which is attached to the moveable steel rods. The movement is controlled by a stepper motor (not shown in this figure), which is situated at the left end of the setup and connected via cogwheels to the steel rods. The whole setup is 1 m long and the source can be moved in a distance from 0.6 cm to 55.6 cm with respect to the PMT. The collimator rings absorb scattered and reflected light from the inner steel wall of the setup. They are arranged in a way that light reflected at the steel wall can not reach the PMT directly.

An in-situ measurement has been performed because the attenuation is strongly dependent on the impurities in the LAr. Light attenuation measurements of other experiments cannot be compared to GERDA due to their different impurity content.

While in the data it is not possible to distinguish between absorption and scattering, but only the attenuation length $1/\alpha_{\text{att}} = 1/\alpha_{\text{abs}} + 1/\alpha_{\text{scat}}$ can be measured, it is necessary to implement absorption and scattering independently into the corresponding simulation. The data that was taken as well as the analysis will be discussed in the following chapters.

2. Experimental setup

For the measurement of the attenuation of the scintillation light in the LAr inside GERDA a dedicated setup was designed that could be deployed directly into the LAr cryostat. A CAD drawing of the setup is shown in figure 1.

The setup consists of a steel tube with a PMT mounted on one end of the tube and a 7 kBq ^{90}Sr source in the volume in front of the PMT, which is held by movable steel rods. The total length of the setup is 1 m and the source can be moved by the steel rods in order to measure the scintillation light in a distance from 0.6 cm to 55.6 cm between PMT and source. The measurement took place at 12 different adequate distances with scaled steps like shown in figure 5.

The β particles emitted by the source deposit energy in the LAr and trigger scintillation light which can be read out by the PMT. As shown in figure 2, ^{90}Sr is an almost pure β emitter, which is essential for this measurement, because gammas can travel very far in LAr, while betas create a nearly point like source of scintillation light. In order to minimize the uncertainty of the distance traveled by the scintillation photons to the PMT, their creation needs to be as point-like as possible.

Since the scintillation light is attenuated during its propagation through the LAr, the measured β spectrum of the ^{90}Sr source looks differently at each distance like shown

in figure 5. Obviously the larger the distance between source and PMT, the less light reaches the PMT.

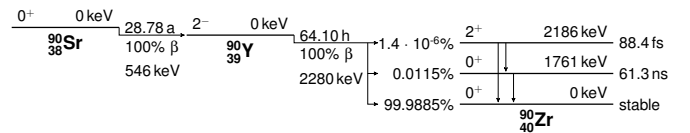


Figure 2: Decay scheme of ^{90}Sr . Values are taken from [6].

A series of stainless steel rings were mounted inside the setup to collimate the scintillation light, blocking photons reflected from the inner steel tube wall. A stepper motor is connected via cogwheels to the steel rods to move the source. All parts of the setup are made of stainless steel, except for the PMT holder, which is made of polytetrafluoroethylene (PTFE). An R11065-10 3" PMT from Hamamatsu is used in the setup. This model was chosen for its low intrinsic radioactivity and its particular design for cryogenic operation. The PMT is coated with the WLS Tetraphenyl butadiene (TPB), in order to shift the scintillation photons (128 nm) to the region where the PMT is sensitive (the peak of the emission spectrum is at 445 nm). Figure 3 shows the LAr scintillation peak, the emission spectrum of TPB and the efficiency curve of the used PMT.

3. Data taking

Pulse traces of the PMT were recorded with a 14-bit Fast Analog to Digital Converter (FADC) board (SIS3301) with a sampling frequency of 100 MHz and a trace length of 131072 samples (approx. 1.3 ms).

All traces were saved for each source position. They were cleaned posteriorly from instrumental backgrounds in order to obtain the photoelectron spectra that is the equivalent to the desired β spectra of the source.

The stepper motor produces a periodic interference with a frequency of about 20 kHz in all the traces.

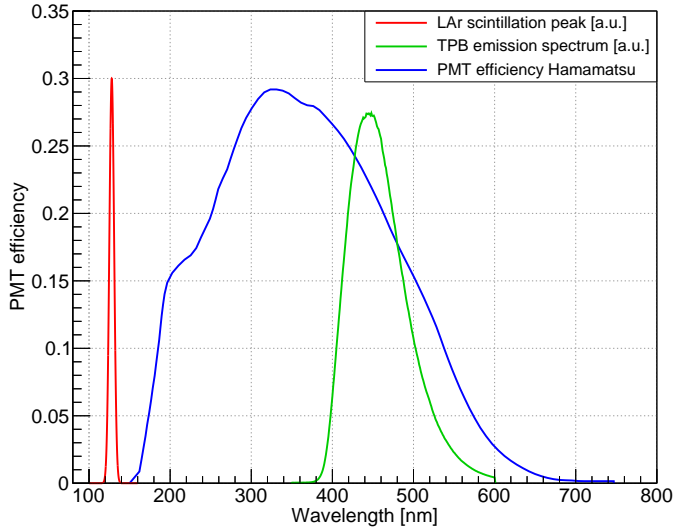


Figure 3: The LAr scintillation light is emitted in a small peak around 128 nm [7] and shifted by TPB [8] to the sensitive region of the PMT [9].

The analysis of an event which is overlaid by a motor interference would falsify the baseline before and after the event as well as the integral of the event. Hence these interferences are flagged in the data cleaning in order to reject events occurring during these interferences in the analysis.

An example trace with flags indicated can be seen in figure 4. Exactly in the middle of every pulse trace is a signal, which exceeds the trigger condition to store the pulse trace. The trigger condition is fulfilled when the sum of two samples subtracted from the sum of the two consecutive samples is larger than 80 ADC channels (see figure 4). This hardware trigger is also not used for the later-on analysis to prevent a systematic bias of larger events, since pulses created by only a few photons cannot

exceed this trigger.

An event can only be found within the unflagged region. The software trigger compares the ADC channel values (see figure 4) of four consecutive samples. The trigger condition is fulfilled when the sum of two samples subtracted from the sum of the following two samples is larger than 20 ADC channels.

The maximal length that is allowed for each event in the analysis is $8 \mu\text{s}$, which corresponds to approximately 4.7 – 8 lifetimes of the triplet state of LAr. There is a 0.03 – 0.9% sacrifice in the signal efficiency due to the mentioned event window cut.

The flagged samples before each motor interference prevent that long events start in the unflagged region and run into the motor interference. Such events would have to be discarded. This would happen more often for long events than for shorter ones, leading to a systematic bias of throwing away more longer events. Therefore, the flagged region before each motor interference is $9 \mu\text{s}$ long, separated into $8 \mu\text{s}$ for pulse reconstruction and $1 \mu\text{s}$ for baseline determination after the event. The flagged region after each motor interference is $1 \mu\text{s}$ for baseline determination before the event.

While the position of the baseline before the event is fixed with no gap to the event, the position of the baseline after the event can be moved by a maximum of $10 \mu\text{s}$, if the baseline is not smooth enough right after the event finished. This is done in order to accept more events with bad or wiggling baselines shortly after the event.

The samples before and after the periodic interference from the stepper motor can be used for pulse reconstruction and baseline determination but a trigger has to lie within the unflagged region (see figure 4).

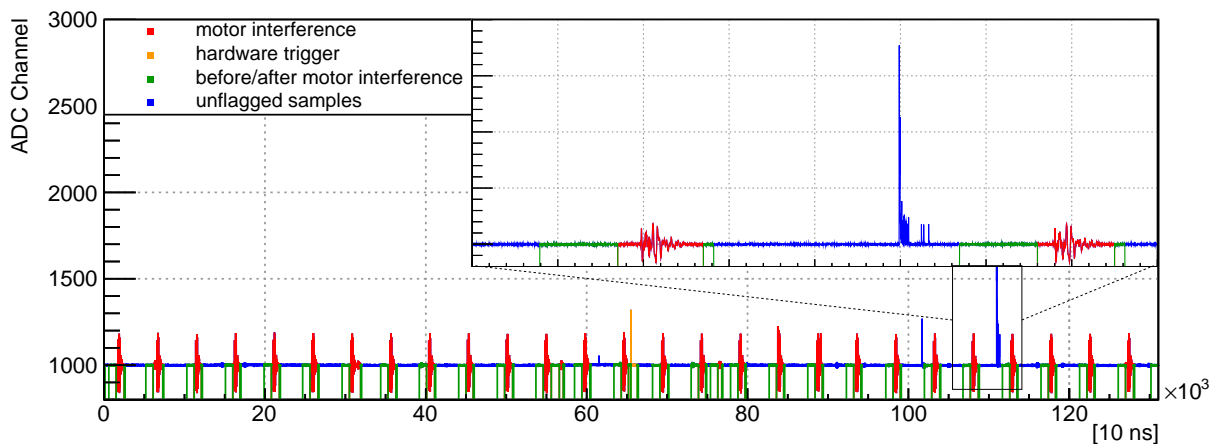


Figure 4: Pulse trace with flags indicated in the overlapping region and the motor interferences. The hardware trigger is flagged in order to avoid a systematic bias of larger events. Only the blue samples are regarded for finding events in the analysis, the green samples can be used for event reconstruction and baseline determination. Events can start in the blue and finish in the blue or green area as long as there are enough samples available for baseline determination before and after the event.

Events starting in the unflagged area, which enter the area before the motor interference, but end at least $1 \mu\text{s}$ before the motor interference starts, will be accepted for further analysis. Events running into or starting within a motor interference can be identified but will be discarded. If the variance of the baseline is small enough, an event will be integrated and the baseline is subtracted from the integral. The integral will enter a histogram as shown in figure 5.

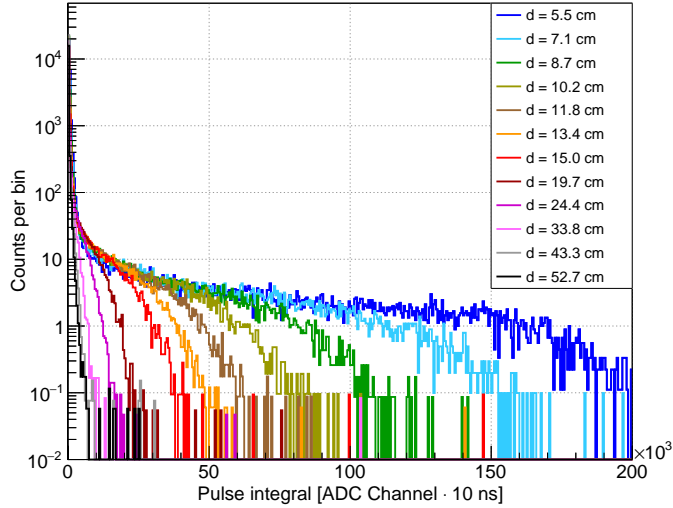


Figure 5: Pulse integral spectra of the ^{90}Sr source for various distances, normalized on the life time of the detector and the ratio of accepted vs. found events.

In order to determine the number of photons in one event, an integration is performed from the beginning of the first pulse until the last pulse of the event with a maximum length of the integration window of $8 \mu\text{s}$. The integrals of all events enter a histogram. The total photon rate is calculated as the histogram which is divided by the life time of each individual measurement and corrected for rejected events. The latter is achieved with a correction factor c , which is the number of accepted events N_{accepted} divided by the number of found events N_{found} : $c = N_{\text{accepted}}/N_{\text{found}}$.

The average incident photon rate is determined, using the spectra in figure 5 which have to be calibrated and integrated. To remove accidental noise triggers, which form the pedestal indicated in figure 6, the low end of the pulse integral spectrum is fit by a combination of an exponential and Gaussian function for the pedestal and a Gaussian function for the single and double photoelectron (p.e.) peak, respectively, which follows the description in [12].

$$f(x) = \underbrace{e^{p_0+p_1 \cdot x} + p_2 \cdot e^{-\frac{(x-p_3)^2}{2 \cdot p_4}}}_{\text{Pedestal}} + \underbrace{p_5 \cdot e^{-\frac{(x-p_6)^2}{2 \cdot p_7}}}_{\text{single p.e. peak}} + \underbrace{p_8 \cdot e^{-\frac{(x-p_6)^2}{2 \cdot p_5}}}_{\text{double p.e. peak}} \quad (1)$$

A cut to eliminate the pedestal was applied to the local minimum between the pedestal and single p.e. peak, above which real photon signals dominate the dataset. An example of such a fit is shown in figure 6.

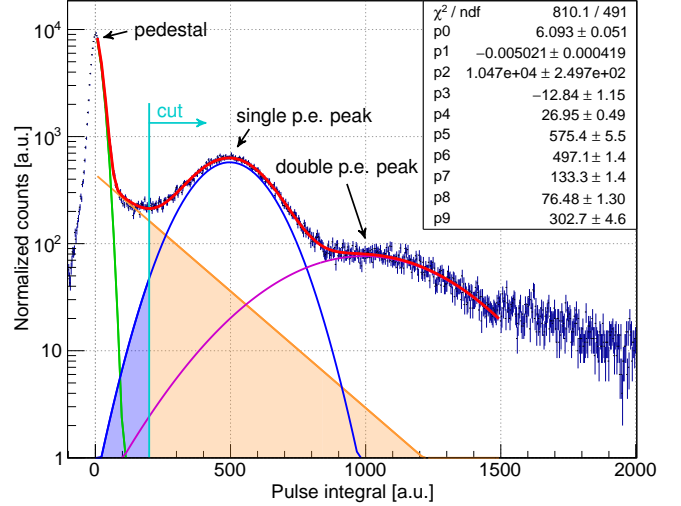


Figure 6: Pulse integral spectrum with the combined fit of the noise pedestal, single p.e. peak and double p.e. peak. The vertical line (light blue) indicates the cut, which is the minimum of the valley between pedestal and single p.e. peak. The spectra is integrated on the right side of this cut. The exponential part (orange) of the pedestal on the right side of the cut is subtracted from the integral and the Gaussian part (dark blue) of the single p.e. peak on the left side of the cut is added to the integral.

The average incident photon rate is calculated by integrating the histogram, weighted by the respective photoelectron value of each bin. Taking the noise into account, this integral is corrected by subtracting the exponential part of the pedestal on the right side of the cut and adding the Gaussian part of the single p.e. peak on the left side of the cut. This integral is proportional to the number of photons that hit the PMT, i.e. the intensity of the light seen by the PMT at the measured distance d . The intensity I of the light follows the Beer-Lambert law:

$$I(d) = I(d_0) \cdot e^{-d/\alpha_{\text{att}}} \quad \text{with} \quad \frac{1}{\alpha_{\text{att}}} = \frac{1}{\alpha_{\text{abs}}} + \frac{1}{\alpha_{\text{scat}}} \quad (2)$$

The attenuation length is denoted with α_{att} , which is composed of the absorption length α_{abs} and the scattering length α_{scat} .

Equation 2 does not include any background light source, but since the ^{90}Sr source can create Cherenkov light inside the LAr an additional term must be added to the background for this measurement. This will be determined by Monte Carlo simulations of the setup.

4. Simulation of the data

A full Monte Carlo simulation of the setup was performed in order to determine the signal and the background measured by the PMT and to test the analysis procedure on simulation data.

4.1. Rayleigh scattering

Calculations and former measurements of the scattering length of LAr can be found in Ref. [13, 14]. However, there is a small discrepancy between the obtained values, the calculation results in 90 cm, while 66 ± 3 cm were measured. A scattering length of 70 cm in LAr for a 128 nm scintillation photon is implemented in the simulation studies for the attenuation measurement in GERDA following the description in [13] and [15]. It should be noted, that the scattering length strongly changes over the width of the 128 nm emission peak of the scintillation light, in fact it is 43 cm at 122 nm and increases to 104 cm at 134 nm.

4.2. Background contribution to the data taking

All relevant background sources have to be implemented into the simulation to improve the match between the model and the measured data. A known background inside the LAr in GERDA is coming from ^{39}Ar , which has an activity of roughly 1.4 Bq/l [16]. ^{39}Ar is a pure beta emitter with an endpoint energy of 565 keV, which is equivalent to a maximum CSDA (continuous slowing down approximation) range for electrons of 2 mm in LAr and 0.4 mm in steel³ [17]. The thickness of the steel tube of the setup is 2.6 mm, hence it is not expected that any ^{39}Ar outside of the setup can contribute to the scintillation light detection. The setup itself contains roughly 71 of LAr, resulting in about 10 Bq of ^{39}Ar that can produce scintillation light inside the setup. Compared to the activity of 7 kBq of the ^{90}Sr source the contribution of ^{39}Ar is negligible.

Another background can originate from the setup itself. It is entirely made out of stainless steel (SAE 304). Measurements of the radiopurity of various kinds of steel are summarized in [18]. A conservative estimation of these measurements does not exceed 3 Bq/kg and the setup weights roughly 13 kg, showing that the background from steel can be neglected as well. Since both are insignificant, background coming from LAr or steel are not considered in the simulation.

The source that is used to trigger the scintillation light is made of ^{90}Sr which decays into ^{90}Y as shown in figure 2. The maximum energy an electron can have from this decay chain is 2280 keV. The minimum energy of electrons to produce Cherenkov light inside LAr is about 260 keV for the creation of an optical photon, but only 150 keV for a photon of 115 nm wavelength. The reason for this is the refractive index which grows with smaller wavelengths. The

refractive index of LAr is implemented in the simulation based on the measurements in [15] and extrapolated down to 110 nm.

Since Cherenkov light is created continuously over a wide wavelength range [19] it is an important background for the attenuation length measurement of the scintillation light. While the WLS shifts UV photons to the optical region, it is transparent to optical photons. Additionally, photons in the optical region have a much longer range in LAr than UV photons, since their energy is too low to excite argon atoms. Furthermore, the reflectivity of steel is different for UV and optical photons, as discussed in chapter 4.3, which increases the traveled path of optical photons in LAr, since they are less often absorbed at the steel surface of the setup in the attenuation measurement. In conclusion Cherenkov light provides a non-trivial and non-constant background with respect to the various distances between PMT and source.

4.3. Reflectivity of the steel

Reflections at the electropolished steel surface of the setup have to be taken into account to determine an effective solid angle correction, which is especially important for Cherenkov light. The reflectivity of the steel of the setup has been measured between 200 nm and 800 nm in the Leibniz Institute of Polymer Research Dresden (IPF) with a Cary 5000 spectrophotometer. The device is not able to measure at lower wavelengths, hence the reflectivity below 200 nm is assumed for the simulation. The measured values as well as the assumptions for the simulation are shown in figure 7. Which reflectivity assumption is used in the simulation is indicated by the reflectivity at 128 nm in the following.

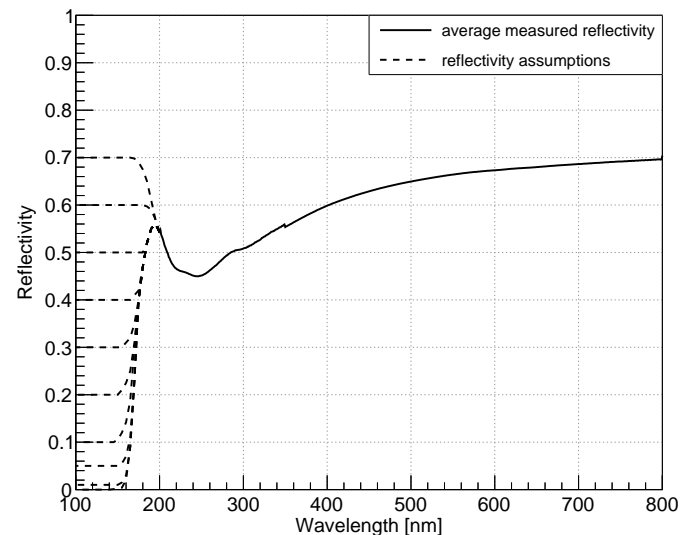


Figure 7: Reflectivity measurement of the electropolished steel between 200 nm and 800 nm. The values below 200 nm must be assumed for the implementation in the simulation.

³Since the material steel is not available in the ESTAR program, the values for iron, nickel and chromium were used for an estimation.

4.4. Solid angle correction and Cherenkov background

To determine the attenuation length from equation 2, a solid angle correction has to be applied to the light intensity measured at each distance. Dedicated simulations were performed to investigate the solid angle correction which is influenced by several effects making it non-trivial.

First of all, the electrons from the ^{90}Sr source can travel a few millimeters in the LAr and produce scintillation photons on their path. Additionally, it is also possible that an electron creates a bremsstrahlung photon which triggers further electrons via Compton scattering or photoeffect farther away from the ^{90}Sr source. This makes the creation of scintillation photons anything but point-like.

A wavelength shifted photon can be emitted away from the PMT, travel through the LAr and can reach the PMT via reflections or scatterings. But since such a photon is in the optical region, where the reflectivity of the steel is high (fig. 7), it can travel a very long distance in LAr and still reach and trigger the PMT.

Furthermore, photons can be reflected at the steel of the setup or Rayleigh scatter inside the LAr which both elongates their traveled distance and increases the distance uncertainty. This is especially important for Cherenkov photons, since the reflectivity is much higher in the optical region (fig. 7) where the PMT is more sensitive as well (fig. 3).

With the help of detailed Monte Carlo simulations it was found, that the solid angle correction is dependent on the reflectivity assumption at 128 nm, as shown in figure 8. As a result the following analysis is performed depending on the reflectivity used in the respective simulation.

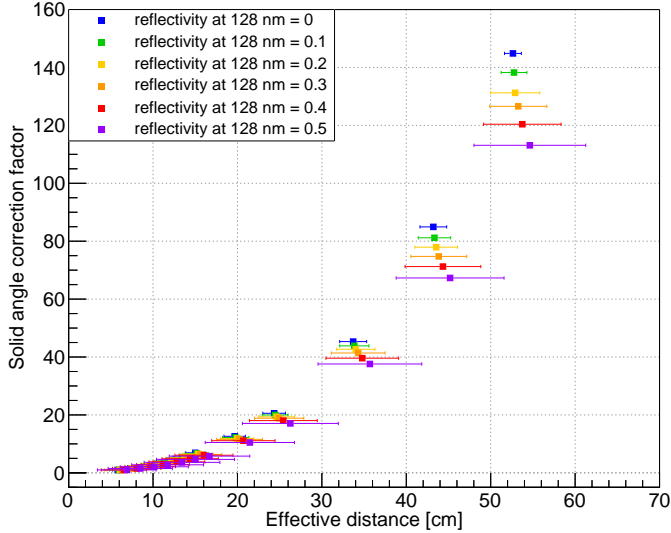


Figure 8: Dependency of the solid angle correction factor on the reflectivity at 128 nm using 6 different values. The simulation data is produced with an absorption length of 1 km, scattering length of 70 cm and a light yield of $5000 \gamma/\text{MeV}$. The uncertainty on the distance grows with the reflectivity because more photons can travel a longer path in LAr since they have a lower probability to get absorbed at the steel surface of the setup.

As it is not possible to distinguish in the data which PMT hits were originated by scintillation photons or Cherenkov photons, all PMT hits will be solid angle corrected. Hence, also the Cherenkov background is dependent on the reflectivity at 128 nm. In order to be able to include the Cherenkov background in equation 2 for a combined fit of signal and background, an analytical description of the Cherenkov background is required. The following fit formula (eq. 3) was found best to describe the Cherenkov background for the respective case of the reflectivity at 128 nm. Figure 9 shows an example of the Cherenkov background fit with equation 3. The Cherenkov background relative to the first measuring point is denoted with b and the distance difference between the measuring points is indicated by Δd .

$$b(\Delta d) = p_0 + p_1 \cdot \Delta d + p_2 \cdot \Delta d^2 + p_3 \cdot \Delta d^3 \quad (3)$$

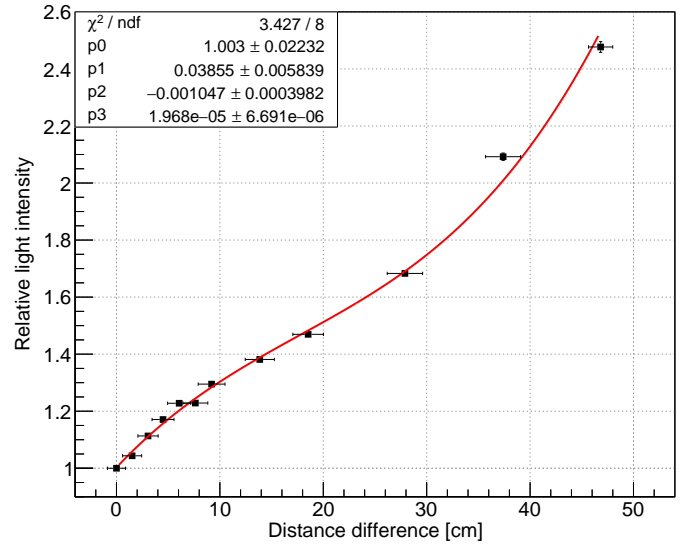


Figure 9: Polynomial fit of the solid angle corrected Cherenkov background for a reflectivity of 0% at 128 nm. The number of Cherenkov hits in the PMT are normalized to the first measuring point and plotted over the distance difference Δd to the first point. Due to the high reflectivity of the steel in the optical region the solid angle corrected Cherenkov background increases with the measuring distance.

4.5. Analysis of the simulation data

To probe the following analysis a series of simulation data was generated with different sets of input parameter values in order to cover a lot of combinations that could be realized in this measurement. For this the absorption length was varied within 10 – 30 cm, the LAr light yield between 1000 – 10000 γ/MeV and the reflectivity at 128 nm was modified like shown in figure 7. These simulations were then analyzed using the same algorithms as for the real data aiming to recover the original input values.

The combined fit $f(\Delta d)$ includes the signal s coming from the scintillation photons and the background b from the Cherenkov light. The fit of the Cherenkov background (eq. 3) is performed beforehand and enters the combined fit with its parameters fixed. Equation 4 shows the combined fit formula and figure 10 the application on two examples of simulation data using:

$$f(\Delta d) = s_{\text{rel}} \cdot s(\Delta d) + (1 - s_{\text{rel}}) \cdot b(\Delta d) \quad (4)$$

$$s(\Delta d) = e^{-\Delta d / \alpha_{\text{abs}}}. \quad (5)$$

The fit parameter s_{rel} reveals the signal strength relative to the sum of signal and background. It gives an indication of the LAr light yield, hence a high value means that the light yield, i.e. the number of produced scintillation photons is high compared to the produced Cherenkov light. Physical results for the parameter s_{rel} have to be between 0 and 1. The parameter α_{abs} gives the absorption length in cm.

Figure 10 also shows that if the absorption length is very short and the light yield is very low (bottom), the influence from the Cherenkov effect is very well visible for larger distances, where less scintillation light reaches the PMT. This is expressed as an increase of the relative light intensity with growing distance difference to the first measuring point. On the contrary, for longer absorption lengths and higher light yields (top) the impact from Cherenkov light is not seen at all and the relative light intensity keeps decreasing with growing distance difference.

5. Analysis of the measured data

In this section the analysis technique used for the simulation in chapter 4.5 is applied to the measured data which is in the following shortly labeled as data. For each single reflectivity assumption at 128 nm a respective solid angle correction is obtained and the data is analyzed with each solid angle correction and afterwards the same fit like for the simulation is applied to the data.

5.1. Search for a simulation model agreeing with the data

With the help of the two fit parameters s_{rel} and α_{abs} from equation 4 a simulation that matches the data best is searched for with a χ^2 -method. By iterative steps of changing the absorption length between 10 – 30 cm and the light yield between 1000 – 10000 γ/MeV , the best matching simulation parameters, i.e., absorption length and light yield, are determined for each reflectivity model.

Since the reflectivity of steel at 128 nm is unknown and the solid angle correction depends on it, it is investigated how the fit parameters s_{rel} and α_{abs} behave if a solid angle correction of a certain reflectivity is applied on simulation data with a different reflectivity.

For this purpose the respective best matching simulations for each reflectivity model are analyzed with every solid angle correction available for each reflectivity assumption.

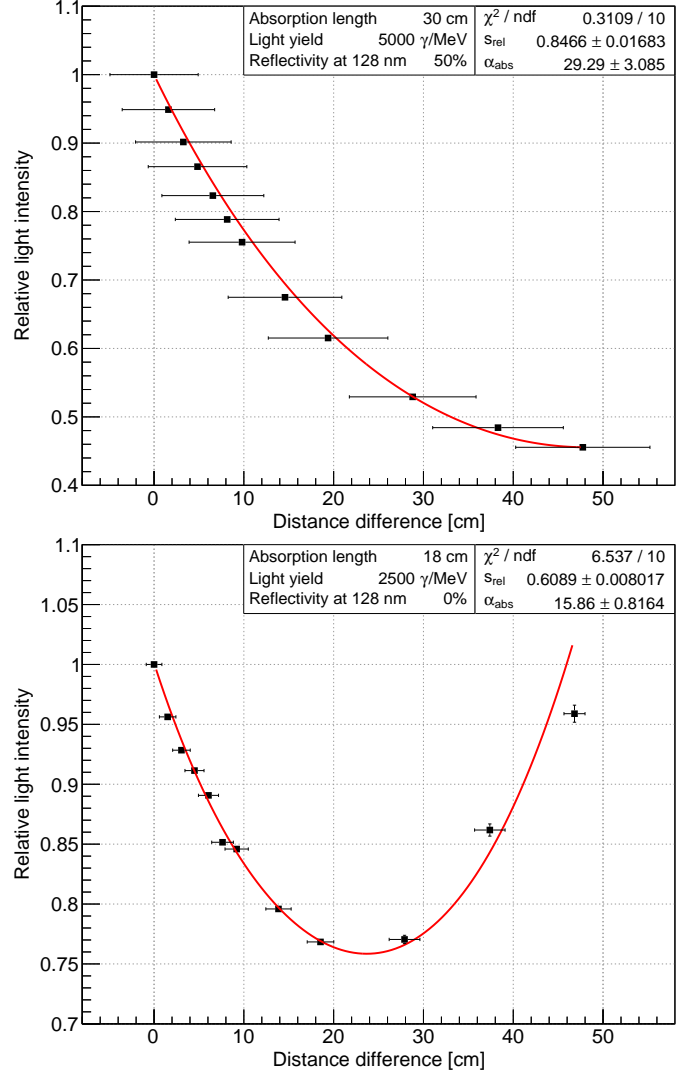


Figure 10: Number of scintillation photons detected by the PMT relative to the first point and combined fit of signal and background for two simulations with various input parameters. In the upper plot no influence from Cherenkov light is visible at all while in the lower plot Cherenkov light is dominating at the longer distances and the relative light intensity grows which is mainly due to the different values of the light yield. With a higher reflectivity (top) photons get less often absorbed at the steel surface, which leads in average to a longer traveled distance and is increasing its uncertainty.

Figure 11 shows the values for the fit parameters s_{rel} and α_{abs} for all cases of simulations analyzed with different solid angle corrections.

The relative signal strength s_{rel} is correlated to the light yield in the simulation data and decreases slightly while increasing the reflectivity of the applied solid angle correction model. The absorption length α_{abs} tends to underestimate the input value of the generated simulation data when analyzing it with a solid angle correction model with a low reflectivity. The fit value of α_{abs} converges to the input value for higher light yields and higher reflectivities in the generated simulation, since the influence of the Cherenkov background decreases in these cases.

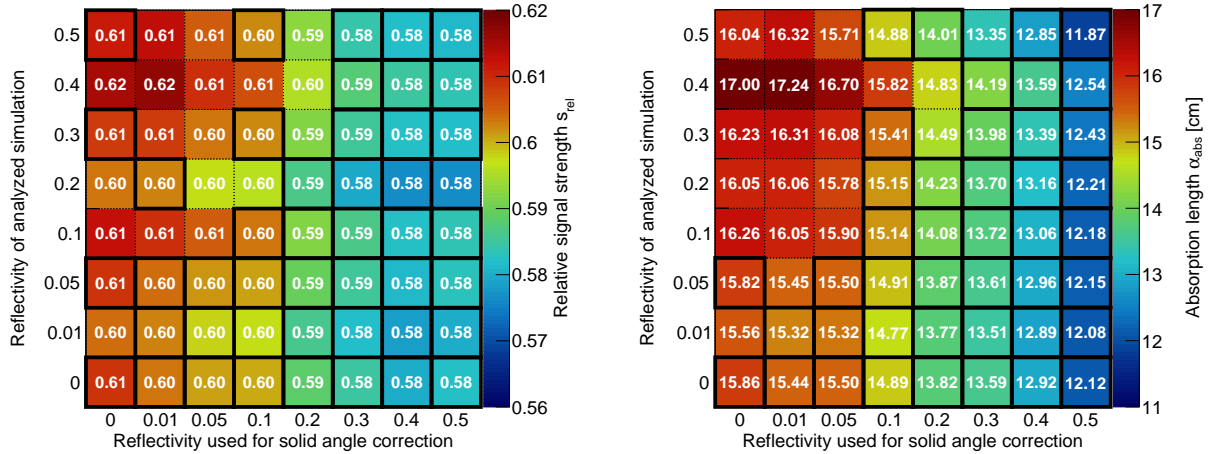


Figure 11: Values for fit parameters s_{rel} (left) and α_{abs} (right) for the best matching simulations of each reflectivity assumption analyzed with solid angle corrections of all reflectivity assumptions. The black boxes mark the values of s_{rel} and α_{abs} that match with the data fit values within 0.32σ uncertainty. The value was decreased from 1σ until only one simulation is marked horizontally. A set of simulation data (plotted on the left axis) is looked for that behaves like the data when analyzing with all reflectivity assumptions (plotted on the bottom axis). In the best case it is expected to observe one horizontal line of black marked bins pointing directly to the best matching simulation on the left side. While individually considered a reflectivity below 5% is favored, both plots together agree to a reflectivity of 0% at 128 nm.

5.2. Comparison of simulation and measured data

The data is also analyzed with the solid angle correction for each reflectivity assumption. The black boxes in figure 11 mark the values of s_{rel} and α_{abs} of the simulations that are within 0.32σ uncertainty of the fit parameters of the data analyzed with the respective solid angle correction. The goal is to find one simulation that behaves exactly like the data when analyzing it with the different solid angle corrections.

As figure 8 already indicates, the uncertainty on the distance grows with a higher reflectivity at 128 nm, because photons are reflected more often and can reach the PMT by longer routes, which increases their average traveled path and also leads to a raise of its uncertainty. This increase in the uncertainty propagates onto the parameters s_{rel} and α_{abs} , whereas the effect is more stronger on α_{abs} . This is the reason why all simulations are marked as matching to the data for high reflectivity assumptions for the solid angle correction in figure 11.

From the plots in figure 11 it can be seen, that the relative signal strength s_{rel} favors the reflectivity models at 0% and 5% and the absorption length α_{abs} at 0%, which is consistent with each other. This means that the best matching simulation for a reflectivity of 0% at 128 nm with an absorption length of 18 cm and a light yield of $2500\gamma/\text{MeV}$ and is behaving like the data when applying solid angle corrections of different reflectivity assumptions.

When comparing the fits of data and simulation directly, the simulation for zero reflectivity at 128 nm matches with the data very well. Both fits are shown in figure 12. Even if the simulation does not match the data at every measuring point perfectly it describes the same trend and the fit results are almost equal.

One reason, that the data points scatter much more than the simulation points could be, that the stepper motor which changed the distance between PMT and source was tested in air to measure the adjusted distances. This does change certainly in LAr due to the low temperature. The shrinkage of the steel setup is about 0.3% from room temperature down to 88 K [22], which reduces the adjusted distance by 1.6 mm for the largest measuring point. In addition to that the source was moved up and down the whole way several times in LAr and the amount of steps the motor needed for the whole range were noted, which leads to an average uncertainty of 1.3 mm in the source movement. Together with the absolute distance uncertainty of 1 mm from the measurement of smallest possible distance this leads to a distance uncertainty for the smallest measuring point of 2.4 mm and for the largest measuring point of 3.9 mm. Hence, the distance adjustment in the measurement can contribute to a larger spread of the measuring points.

5.3. Results and discussion

The attenuation measurement in the GERDA LAr cryostat results in an absorption length of

$$\alpha_{abs} = 15.79 \pm 0.70(\text{stat})_{-3.14}^{+1.42}(\text{syst}) \text{ cm} \quad (6)$$

with the assumption of a scattering length of 70 cm at 128 nm and a reflectivity of steel of 0% at 128 nm.

The systematic uncertainty is obtained by analyzing the measured data with various solid angle correction models generated with different parameter values and calculating the difference of the results to equation 6.

The following parameters were modified with respect to their default values: the steel reflectivity at 128 nm was increased from 0% to 5%, the effective area of the PMT was changed from the minimum to the maximum possible diameter, the scattering length at 128 nm was set to the values derived from the width of the scintillation peak like described in chapter 4.1 and the distance between PMT and source was changed according to the uncertainty of the distance adjustment of the stepper motor and the shrinkage of the setup due to the operation in LAr. The investigated systematics with the respective difference to the resulting absorption length are listed in table 1.

With equation 2 this leads to an attenuation length of $12.88 \pm 0.50(\text{stat})_{-2.24}^{+1.01}(\text{syst})$ cm in the LAr in GERDA with the assumption of a scattering length of 70 cm at 128 nm.

Table 1: Simulation parameters for the investigation of the systematic uncertainties and the resulting difference to the absorption length quoted in equation 6.

| simulation parameter | syst. uncertainty |
|---------------------------------|-------------------|
| reflectivity at 128 nm | -0.39 cm |
| efficient area of the PMT | -2.73 cm |
| scattering length at 128 nm | +0.19 -0.52 cm |
| distance between PMT and source | +1.41 -1.42 cm |

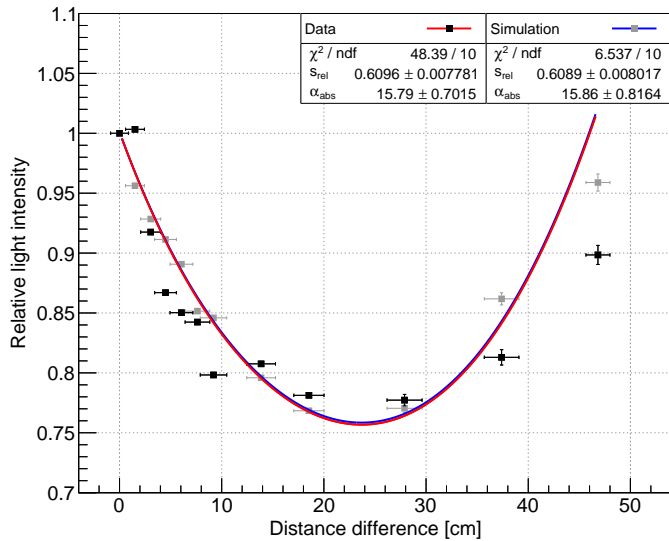


Figure 12: Comparison of data and best matching simulation analyzed with the solid angle correction of a reflectivity assumption of 0% at 128 nm. The simulation data was generated with an absorption length of 18 cm, a light yield of 2500 γ/MeV and a reflectivity of 0% at 128 nm.

The major contribution to the uncertainty on the fit result of the absorption length as shown in figure 12 is coming from the uncertainty on the effective distance between source and PMT (relative uncertainty: 10.6% for the smallest distance, 1.9% for the largest distance). This is a direct consequence of the path length a scintillation photon travels from its point of origin until reaching the

WLS on the PMT. This uncertainty cannot be reduced by increasing statistics because this would have no effect on the traveled path of the photons. Another contribution to the uncertainty arises from the Monte Carlo statistics of the solid angle correction, which gets lower for the measuring points that are further away from the PMT (relative uncertainty: 0.1% for the smallest distance, 0.8% for the largest distance).

6. Conclusions and Outlook

An attenuation length measurement was performed successfully in the GERDA LAr cryostat with a dedicated setup. The attenuation length was determined using simulations to take background, geometrical effects and interactions during the light propagation into account. A set of simulation data was generated to cross-check the subsequent analysis which was performed for the data as well. The parameters which result in the best fitting simulation are an absorption length of 18 cm, a scattering length of 70 cm at 128 nm, a light yield of 2500 γ/MeV and a reflectivity of the steel of the setup of 0% at 128 nm. These parameters are compatible with the data.

Comparing our result to other measurements of the attenuation length of scintillation light in LAr [3, 20, 21] the obtained value is much smaller. The result in [20] of about 50 cm is in the same order of magnitude like measured in this work. However in other measurements very pure LAr was taken initially and doped with impurities in order to measure the attenuation dependent on the impurity composition. These measurements with the purest LAr samples result in 1.10 m [21] and in 30 – 1790 m [3]. On the contrary the LAr in the GERDA cryostat is not exposed to any purification plant and dwells in the cryostat already before the start of Phase I of GERDA in 2011.

Despite the fact that the attenuation length and the light yield are very low, the LAr veto performs very well, because almost everything is coated with WLS. Most important is that a photon reaches the WLS and gets shifted in the optical region, because then it has a much longer range in LAr and a higher probability of reaching a PMT. Additionally, Cherenkov light can also be created by background events in the LAr in GERDA and it can be used together with the scintillation light for the LAr veto. In fact it is not possible to distinguish with the LAr veto if a signal in the PMTs came originally from scintillation or Cherenkov photons. However Cherenkov light is created continuously and also in the optical region, hence it has a long range in LAr and therefore improves the efficiency of the LAr veto.

After GERDA finishes Phase II and the detector array is retrieved from the LAr cryostat, the attenuation measurement could be redone to check if the LAr properties changed or stayed the same. It is especially interesting to investigate the LAr quality over time since it is planned to build the successor experiment LEGEND [23] in the same infrastructure.

In principle the setup can be used in other experiments as well to measure noble gas properties like absorption length and triplet lifetime. In fact the PMT and the source can be exchanged to be able to cover other demands, where the used combination of a high energy beta source, the WLS TPB and the PMT designed for low temperature operation are not optimal.

Depending on the density of the liquid in which the setup is operated, the source holder is heavy enough to sink down if it is not held by the stepper motor in its place. The setup could be improved by constructing a mechanical holder which prevents the source holder from moving while the stepper motor is switched off. In this way the interference from the motor occurring in the pulse traces could be completely eliminated which makes the data cleaning more easier and less samples have to be discarded for the analysis. Additionally a pure alpha source could be searched for which can be deployed in LAr. Since alpha particles are too slow to create Cherenkov light in LAr, this would prevent the Cherenkov background in this measurement.

Acknowledgments

This work was supported in part by grants from BMBF, DFG, INFN, MPG, NCN, RFBR and SNF. The authors thank the workshop of TU Dresden for building the setup and the colleagues and the workshop of the MPIK in Heidelberg for the opportunity to test the setup in liquid nitrogen. Additional thanks go to Anja Maria Steiner from the IPF in Dresden who made it possible to measure the reflectivity of the steel. Furthermore we thank the Center for Information Services and High Performance Computing (ZIH) at TU Dresden for the generous allocation of computing power. The GERDA collaboration thanks the director and the staff of the LNGS for their continuous strong support of the GERDA experiment.

References

- [1] M. Agostini et al. (GERDA Collaboration), *Phys. Rev. Lett.* **120**, 132503 (2018)
- [2] A.J. Zsigmond, DOI 10.5281/zenodo.1287603 (2018)
- [3] B.J.P. Jones *et al.*, *Journal of Instr.*, Vol. 8 (2013)
- [4] R. Acciarri *et al.*, *Journal of Instr.*, Vol. 5 (2010)
- [5] B.J.P. Jones *et al.*, *Journal of Instr.*, Vol. 8 (2013)
- [6] The Lund/LBNL Nuclear Data Search
<http://nucleardata.nuclear.lu.se/toi/>
- [7] T. Heindl *et al.*, *Europhys. Lett.* **91** 6 (2010)
- [8] R Francini *et al.* *Journal of Instru.*, Vol. 8, (2013=
- [9] Hamamatsu *Photonic devices* 2015
- [10] M. Agostini et al. (GERDA Collaboration), *Eur. Phys. J. C* **78** (2018) 388
- [11] C. Amsler *et al.*, 2008 JINST **3** P02001
- [12] E.H. Bellamy *et al.*, *Nucl. Instr. and Meth. A* **339**, 468 (1994)
- [13] G.M. Seidel *et al.*, *Nucl. Instr. and Meth. A* **489**, 189 (2002)
- [14] N. Ishida *et al.*, *Nucl. Instr. and Meth. A* **384**, 380 (1997)
- [15] A. Bideau-Mehu *et al.*, *J. Quant. Spectrosc. Radiat. Transfer* **25**, 395 (1981)
- [16] P. Benetti *et al.*, *Nucl. Instr. Meth. A* **574**, 83 (2007)
- [17] ESTAR program by NIST
<https://physics.nist.gov/PhysRefData/Star/Text/ESTAR.html>
- [18] www.radiopurity.org
(accessed 29.10.2018)
- [19] M. Tanabashi et al. (Particle Data Group), *Phys. Rev. D* **98**, 030001 (2018)
- [20] ArDM Collaboration, *Astrop. Phys.*, Vol. 97, P. 186 (2018)
- [21] A. Neumeier *et al.*, *Europhys. Lett.* **111** 12001 (2015)
- [22] E.D. Marquardt *et al.*, *Cryogenic Material Properties Database* (2000)
- [23] LEGEND Collaboration *AIP Conf. Proc.* **1894** (2017) no.1, 020027